Many particle aspects of a semiconductor quantum wire within an improved random phase approximation

2005 J. Phys.: Condens. Matter 17 3043

(http://iopscience.iop.org/0953-8984/17/19/018)

INSTITUTE OF PHYSICS PUBLISHING JOURNAL OF PHYSICS: CONDENSED MATTER

J. Phys.: Condens. Matter **17** (2005) 3043–3059 doi:10.1088/0953-8984/17/19/018

Many particle aspects of a semiconductor quantum wire within an improved random phase approximation

S S Z Ashraf and A C Sharma

Physics Department, Faculty of Science, The MS University of Baroda, Vadodara-390 0002, India

Received 31 December 2004, in final form 10 March 2005
Published 29 April 2005
Online at stacks.iop.org/JPhysCM/17/3043

Abstract

The structure factor, pair distribution function, screened impurity potential, density of screening charge, and exchange and screened exchange energies have been theoretically investigated for a semiconductor quantum wire using an improved random phase approximation that takes into account the local field corrections within the Hubbard approximation. Our approach enabled us to obtain approximate analytical results on some of the aspects and to greatly simplify the computation task on others. However, computed results from our simple approach show very good agreement with those obtained by performing cumbersome numerical solutions for the structure factor, density–density response function and the static local field corrections, within the Singwi–Tosi–Land–Sjölander approximation. Our investigations suggest that: (i) the magnitude of the screened impurity potential and the average distribution of electrons about an electron at larger distances are enhanced on reducing the width of quantum wire, and (ii) the exchange interactions strengthen on narrowing the quantum wire and on increasing the carrier density. Friedel oscillations are seen in both our computed screened potential and the density of screening charge.

(Some figures in this article are in colour only in the electronic version)

1. Introduction

Many body effects play an important role in one-dimensional electron gas (1DEG), quasi-1DEG and two-dimensional electron gas (2DEG) because of severe restrictions in the phase space. There have been several attempts to understand the many body aspects of 1DEG and 2DEG [1–11]. Various approximations such as the Thomas–Fermi approximation (TFA), the random phase approximation (RPA) and the improved RPA (IRPA) that incorporate local field corrections (LFC) have been employed to study the effect of many body interactions on the properties of 1DEG and 2DEG. In the case of 1DEG, certain properties such as plasma oscillations can be very well understood within RPA, while RPA gives grossly unphysical

results on some of the ground state properties such as the pair-correlation function and self-energy. The ground state properties of 1DEG and 2DEG have been investigated beyond RPA by taking into account the LFC through approximations such as the Singwi–Tosi–Land–Sjölander (STLS) approximation. The phenomenon of screening and the many body aspects (MBA) that involve screening are the simplest and most important manifestations of electron–electron interactions. Also, the screening is a phenomenon influencing and even determining much of the physical world, from cosmic plasmas to lightning propagation, electronic devices, electrochemical machining, biopolymers, membranes and neuronal activity, and therefore has an application to materials science, chemistry and biology. In addition to electron scattering from disorder/impurity, screening of the electron–electron interaction is one of the most important effects that make possible the use of the free electron or quasi-particle model in describing the properties of 1DEG and 2DEG [12, 13].

It is widely believed that the properties of interacting 1DEG can be better described within the Tomonaga–Luttinger (TL) model, where elementary excitations are of bosonic character rather than the Fermionic nature encountered in Fermi liquid (FL) [14–16]. However, there have been very few convincing experimental demonstrations of TL liquid in real 1DEG or quasi-1DEG systems, despite intensive theoretical interest [17–21]. Contrary to what one might expect based on the well-established TL model theoretical projections, the experimental data obtained on 1D structures from measurements on photoluminescence, inelastic light scattering (Raman scattering), far infrared spectroscopy, capacitance studies, etc, can be successfully explained on the basis of normal 1D FL theory [4, 22]. This fact is also endorsed by the success of other theories, such as the Landauer–Buttiker formula that treats electrons in mesoscopic quasi 1D systems as non-interacting entities [23]. These arguments suggest that ordinary FL theory is valid in the presence of impurity scattering, which always exists (however weak it may be), in a real 1D electron system at finite temperature. The decay time of single electron excitation is important for the resurrection of the FL theory and it also determines the magnitude and temperature dependence of the quantum corrections to the conductivity. The excitations decay more rapidly when there is disorder in a system.

The dielectric function (DF) formalism of a solid leads to theoretical understanding of various MBA such as screening of the impurity potential, optical properties, collective excitations, exchange and correlation energy, self energy, static structure factor $S(q)$, pair-distribution function $g(r)$, LFC and density of screened charge $n_s(r)$. $\boldsymbol{q}$ and $\mathbf{r}$ are the wavevector and position vector, respectively. The $g(r)$ is an average distribution of electrons about any electron in a solid, and it is defined as the probability that another particle is at position $\mathbf{r}$ if there is already one at $\mathbf{r} = 0$. The screened potential (SP) about a point charge diverges for $\mathbf{r} \to 0$, as do all coulomb potentials. However, the $n_s(r)$ about a point charge impurity can remain finite even at the origin $r = 0$. The DF models based on TFA, RPA and IRPA explain successfully, but not completely, the phenomenon of screening and MBA of 3D electron gas [24–26]. This led to the recent interest in probing theoretically the phenomenon of screening and MBA under novel conditions, in 1D and 2D electron gas with the use of RPA and IRPA. The manner in which mobile charge carriers interact with each other and shield the bare coulomb potential depends on the dimensions of the system and a reduction in the dimensionality of the system reduces the screening effects. More elaborately the screening is weaker in 1D than in 2D, which in turn is weaker in comparison to 3D electron gas. The screening cloud in 2D is confined to the plane of the layer and cannot surround the external charge as perfectly as in 3D and similarly in 1D the Fermi surface consisting two planes at $\pm k_F$ cannot shield the external charge as effectively as in the case of 2D and 3D. k_F is a Fermi wavevector.

Recently, there have been theoretical studies of the behaviour of the SP for a small wavevector using TFA [24], and of MBA with the use of IRPA [1–3, 10, 11], for a quantum wire

(QW). The TFA results exhibit an unphysical divergence in the electron density as $\mathbf{r} \to 0$, and they are found inadequate to reproduce the oscillations called the Friedel oscillations resulting from the abrupt change in screening at a wavevector equal to $2k_F$. These oscillations dominate the long-range behaviour of SP, which is a direct result of the sharpness of the Fermi-distribution, and states with $k > k_F$ are unoccupied while those with $k < k_F$ are filled at $T = 0$. These oscillations have been found to occur in 3D, 2D and 1D systems at low temperatures. In 1D and quasi-1D systems, the intrinsic energies involved are comparable to the experimental temperature and the TFA, which is analogous to the small wavevector limit of RPA results, can hold good to a reasonable degree. However, in a 1D electron gas or a semiconductor QW, the plasmon dissipation goes to zero as the momentum q gets smaller and the dynamical effects become prominent. These low energy virtual plasmon excitations can be crucial in dynamical screening, as the elementary excitations here are different from those of non-interacting systems. To include plasma effects and the long-range oscillations it is desirable to go over the TFA and study the screening effects within the RPA or IRPA. The past studies on $S(q)$, $g(r)$, exchange and correlation energy, compressibility and $n_s(r)$ for 1D and quasi-1D electron gas have been performed using IRPA that incorporates the LFC in the self-consistent STLS approach [1–3, 10]. These calculations include static as well as dynamical LFC and they are claimed to be very close to Monte Carlo findings. However, simultaneous numerical solutions of equations for $S(q)$, LFC and the density–density response function $\chi(q, \omega)$ are to be performed in these studies, which is a heavy computational task. No analytical results on any of the MBA are possible within the STLS approach and the numerically computed results lack convincing simplicity. This motivated us to perform a theoretical study on the MBA of QW using the IRPA that incorporates LFC and the essential physics of 1D electron gas in a simple manner. We aim to obtain approximate analytical results on some of the physical properties and to simplify the computational task on many others. Our approach incorporates the LFC within the Hubbard approximation (HA) to describe the particle–particle interaction in a simple manner. The necessary formalism used in our work is given in section 2. Results and the subsequent discussions on them are reported in section 3 and finally the work is concluded in section 4.

2. Model and essential formalism

We consider an electron gas with δ-function type confinement along the z-axis and an infinite potential well type confinement along the y-axis. We assume that the electron wavefunction vanishes at boundaries of the wire across the y-axis, at $y = \pm a/2$, where a is the width of a QW. It is further assumed that electrons perform unrestricted motion along the x-axis and the band for motion is parabolic; $\xi_k = \frac{\hbar^2 k^2}{2m^*} - \mu$, where m^* is the effective electron band mass and μ is the chemical potential. This is a reasonable assumption for a QW where electron density is low ($\sim 10^6$ cm^{-1}), occupying only the lowest (ground) subband. The bare coulomb potential, $V^0(q)$, for a QW is given by [27, 29]

$$V^0(q, y, y') = \frac{2e^2}{\varepsilon_0} k_0(q|y - y'|), \tag{1}$$

where q is a 1D wavevector and ε_0 is the background dielectric constant. The $k_0(q|y - y'|)$ is the zeroth order modified Bessel function, which can be defined as [27]

$$k_0(q|y - y'|) = \int_0^\infty \mathrm{d}t \, \frac{\exp(-|y - y'|\sqrt{t^2 + q^2})}{\sqrt{t^2 + q^2}}. \tag{2}$$

The evaluation of $V^0(q)$ with the use of equations (1) and (2) yields

$$V^0(q) = \frac{2e^2}{\varepsilon_0}\int_0^\infty \mathrm{d}t\,\frac{H(\lambda)}{\lambda}, \tag{3}$$

with

$$\lambda = \sqrt{t^2+q^2}. \tag{4}$$

The $H(\lambda)$ is defined as

$$H(\lambda) = \int_{-a/2}^{a/2}\mathrm{d}y\int_{-a/2}^{a/2}\mathrm{d}y'\,\exp(-\lambda|y-y'|)|\phi(y)|^2|\phi(y')|^2. \tag{5}$$

Evaluation of equation (5) by taking envelope functions $\phi(y)$ and $\phi(y')$ that vanish at $y = \pm a/2$ gives [28]

$$H(\lambda) = \left(\frac{u}{w}+\frac{2}{u}\right) - \frac{32\pi^4}{(wu)^2}(1-\mathrm{e}^{-u}), \tag{6}$$

where $u = \lambda a$ and $w = u^2+4\pi^2$. For larger values of a ($u \gg 2\pi$), $H(u) \to 3/u$ and $V^0(q)$ reduces to $\frac{3\pi e^2}{\varepsilon_0|qa|}$, which agrees with the asymptotic results on $V^0(q)$ reported elsewhere [29]. By contrast, for smaller values of u ($\ll 1$), $H(u)$ reduces to unity and equation (3) becomes

$$V^0(q) = \frac{2e^2}{\varepsilon_0}\int_0^\infty \frac{\mathrm{d}t}{\sqrt{t^2+q^2}}. \tag{7}$$

The $V^0(q)$ given by equation (7) has also been used to investigate properties of 1D electron gas [25, 28]. The integrand of equation (7) diverges logarithmically at the upper limit when $q \neq 0$ and at the lower limit for $q \to 0$. The divergence at the upper limit was cut off by taking an upper limit, $q_c \approx 1/a$, to obtain $V^0(q)$ that describes well the interactions at distances much larger than a. The integrand in equation (3) has better convergence as compared to that in equation (7), and it does not show logarithmic divergence at the upper limit because $H(u) \to 0$ when $t \to \infty$.

$$V^0(q) = (e^2/\varepsilon_0)\mathrm{e}^x k_o(x), \tag{8}$$

with $x = (qb/2)^2$, where b is the lateral width of QW determined by the confining oscillator frequency; this has also been used in the literature [1, 2]. We find that our equation (3), as compared to equations (7) and (8), gives a better description of the bare coulomb potential for a QW and it is valid at all values of q and a. On the other hand, the validity of equation (8) becomes questionable for a QW of smaller width ($a < 5$ nm).

The quantity of central importance in studying the MBA and screening phenomenon is $\chi(q,\omega)$, defined by

$$\chi(q,\omega) = \frac{\chi_0(q,\omega)}{\varepsilon(q,\omega)} \tag{9}$$

where DF, $\varepsilon(q,\omega)$ is defined as [30, 31]

$$\varepsilon(q,\omega) = 1 - V^{\mathrm{eff}}(q)\chi_0(q,\omega). \tag{10}$$

$\chi_0(q,\omega)$ is the 1D irreducible polarizability function. The effective electron–electron interaction, $V^{\mathrm{eff}}(q)$ is defined by

$$V^{\mathrm{eff}}(q) = V^0(q)[1-G(q)] \tag{11}$$

where $G(q)$ is the static LFC term. There have been several ways to calculate $G(q)$ for 1D electron gas. The HA is the simplest way to incorporate the static LFC. The $G(q)$, within HA, for the 3D electron gas is given by [8, 30]

$$G(q) = \frac{1}{2}\frac{q^2}{q^2 + k_F^2} \equiv \frac{1}{2}\frac{4\pi e^2/(q^2 + k_F^2)}{4\pi e^2/q^2}. \tag{12}$$

In terms of the bare coulomb potential, equation (12) can be rewritten as

$$G(q) = \frac{1}{2}\frac{V^0(\sqrt{q^2 + k_F^2})}{V^0(q)}. \tag{13}$$

For $q \to 0$, $V^{\text{eff}}(q)$ reduces to $V^0(q)$. Equation (13) can also be used to compute $G(q)$ for a QW or 1D electron gas. The $V^0(\sqrt{q^2 + k_F^2})$ is obtained from equation (3) on replacing q by $\sqrt{q^2 + k_F^2}$.

The $\chi_0(q, \omega)$ in a single subband approximation, which is valid when the Fermi energy is much smaller than the intersubband energy difference, is given by [29]

$$\chi_0(q, \omega) = 2\int \frac{\mathrm{d}p}{2\pi}\frac{n_p - n_{p+q}}{\xi_p - \xi_{p+q} + \hbar(\omega + \mathrm{i}\gamma)} \tag{14}$$

where n_p is the Fermi distribution function at $T = 0$ and γ is the damping parameter arising from electron-disorder/impurity scattering. In this paper we consider the case of a QW with a negligibly small amount of disorder (impurity) and therefore we evaluate equation (14) for $\gamma \to 0$. The real and imaginary parts of $\chi_0(q, \omega)$ for $\gamma \to 0$ are given as

$$\chi_{01}(q, \omega) = \frac{m^*}{\pi q}\log\left[\frac{\omega^2 - (E_q - q v_F)^2}{\omega^2 - (E_q + q v_F)^2}\right] \tag{15a}$$

and

$$\chi_{02}(q, \omega) = \begin{cases} \dfrac{m^*}{\hbar^2 q}, & \text{when } |E_q - q v_F| \leqslant \omega \leqslant (E_q + q v_F), \\ 0 & \text{otherwise} \end{cases} \tag{15b}$$

where $E_q = \hbar^2 q^2/2m^*$. We intend to study the following physical quantities in this paper.

2.1. The structure factor and pair distribution function

The $S(q)$ is defined as [1, 30]

$$S(q) = \frac{-1}{n\pi}\int_0^\infty \mathrm{d}\omega\ \mathrm{Im}[\chi(q, \omega)] \tag{16}$$

where Im stands for the imaginary part and n is the number of electrons per unit length. Equation (16), with the use of equations (10) and (15), can be rewritten as

$$S(q) = \int_{\omega_1}^{\omega_2} \mathrm{d}\omega\, S(q, \omega) \tag{17a}$$

where the dynamical structure factor, $S(q, \omega)$, is defined as

$$S(q, \omega) = \frac{-1}{n\pi V^{\text{eff}}(q)}\left[\frac{\varepsilon_2(q, \omega)}{\varepsilon_1^2(q, \omega) + \varepsilon_2^2(q, \omega)}\right]. \tag{17b}$$

$\varepsilon_1(q, \omega)$ and $\varepsilon_2(q, \omega)$ are the real and imaginary parts of $\varepsilon(q, \omega)$, respectively, $\omega_1 = |E_q - q v_F|/\hbar$ and $\omega_2 = (E_q + q v_F)/\hbar$.

The $g(r)$ can be calculated from $S(q)$ through a Fourier transform as follows [1, 30]:

$$g(r) = 1 + \frac{1}{n\pi}\int_0^\infty \mathrm{d}q\, \cos(qr)[S(q) - 1]. \tag{18}$$

2.2. Dielectric function and screened potential

The DF that takes into account the LFC is given by equation (10). The Fourier transformed SP is defined as

$$W(q,\omega) = \frac{V^i(q)}{\varepsilon(q,\omega)}, \tag{19}$$

where $V^i(q) = ZV^0(q)$ is the bare impurity potential in Fourier space. Ze is the charge on impurity. The static screened impurity potential in real space is then obtained by performing a 1D Fourier transform,

$$W(r) = \int_{-\infty}^{\infty} \frac{\mathrm{d}q}{2\pi} W(q)\mathrm{e}^{\mathrm{i}qr}. \tag{20}$$

2.3. Density of the screening charge

The $n_s(r)$ for a QW can be calculated from [1, 30]

$$n_s(r) = Ze\int_{-\infty}^{\infty} \frac{\mathrm{d}q}{2\pi}\,\mathrm{e}^{\mathrm{i}qr}\left[1 - \frac{1}{\varepsilon(q)}\right]. \tag{21}$$

2.4. Exchange energy and IRPA self-energy

The wavevector dependent exchange energy, within the IRPA, is given by [30]

$$E^{\mathrm{xc}}(k) = \int_{-k_\mathrm{F}}^{k_\mathrm{F}} V^{\mathrm{eff}}(|\mathbf{k}-\mathbf{k}'|)\frac{\mathrm{d}k'}{2\pi}. \tag{22a}$$

The screened exchange energy, also called the IRPA self-energy, is defined as [30]

$$E^{\mathrm{sl}}(k) = \int_{-k_\mathrm{F}}^{k_\mathrm{F}} \frac{\mathrm{d}k'}{2\pi}\frac{V^{\mathrm{eff}}(|\mathbf{k}-\mathbf{k}'|)}{\varepsilon(|\mathbf{k}-\mathbf{k}'|)}. \tag{22b}$$

$V^{\mathrm{eff}}(|\mathbf{k}-\mathbf{k}'|)$ and $\varepsilon(|\mathbf{k}-\mathbf{k}'|)$ are obtained from $V^{\mathrm{eff}}(q)$ and $\varepsilon(q,\omega=0)$ on replacing q by $|\mathbf{k}-\mathbf{k}'|$.

3. Results and discussions

The formalism developed in section 2 has been applied to a GaAs-QW, which is parameterized in terms of $m^* = 0.068\,m_\mathrm{e}$ and $\varepsilon_0 = 12.0$ [27, 28]. Before discussing our results, we ensure that the formalism developed in section 2 is correct and conforms to the requirement of the conservation laws: $p' - p = q$ and $\hbar\omega = \xi_{p'} - \xi_p$. It is to be noted that equation (15*b*) has been obtained from (14) by strictly following the momentum and energy conservation laws. We further subject our formalism to the scrutiny of the sum-rules, which are a class of exact results. One of the sum rules that complies with conservation laws is

$$\int_0^{\infty} \varepsilon_2(q,\omega)\omega\,\mathrm{d}\omega = \frac{\pi\omega_\mathrm{p}^2}{2} \tag{23a}$$

where ω_p is the plasma frequency. Evaluation of ω-integration, with the use of equations (10) and (15*b*), transforms equation (23*a*) to

$$\frac{4m^*V^{\mathrm{eff}}(q)}{\hbar^2 v_\mathrm{F} E_q \omega_\mathrm{p}^2} = \pi. \tag{23b}$$

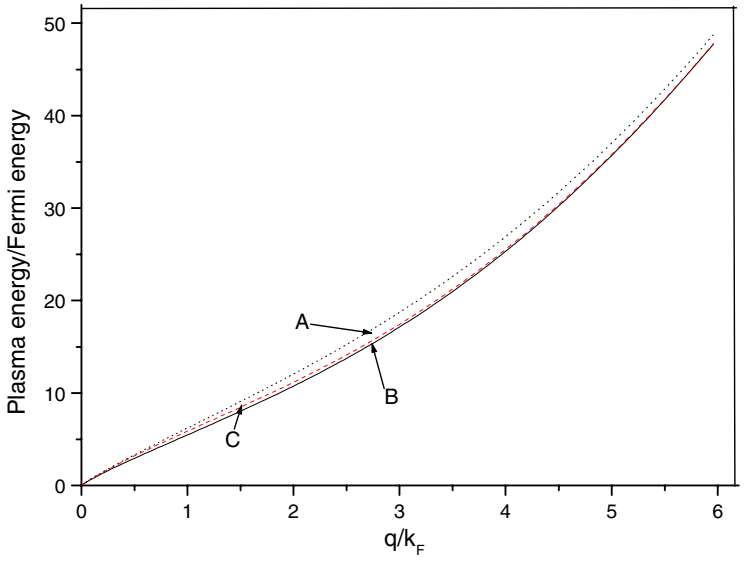

Figure 1. The normalized plasma frequency is plotted as a function of the normalized wavevector. IRPA plasma frequencies at $k_F = 5 \times 10^5$ cm^{-1} for $a = 5$ nm (curve-A) and for $a = 20$ nm (curve-B) are shown by dot–dot and solid lines, respectively. The dash–dash line represents the RPA plasma frequency at $k_F = 5 \times 10^5$ cm^{-1} and $a = 10$ nm (curve-C).

The solution of $\varepsilon_1(q, \omega_p) = 0$ gives

$$\omega_p^2(q) = (E_q + q v_F)^2 + 4E_q q v_F/(A - 1), \tag{24}$$

with $A = e^{\pi q \hbar^2/m^* V^{\rm eff}(q)}$. For smaller values of $q(<0.1k_F)$, $\omega_p^2(q)$ can be approximated by $4m^* V^{\rm eff}(q)/\pi\hbar^2 v_F E_q$ that exactly satisfies equation (23*b*). However, the fulfilment of (23*b*) with the use of (24) is at stake when q increases. As is seen from equation (23*b*) and figure 1, $\omega_p^2(q)$ with LFC is smaller than that without LFC, at all values of q. This suggests that incorporation of LFC in the scheme extends the range of q-values over which sum-rules can be satisfied and that the range is determined by the value of $G(q)$. We checked the compliance of other sum-rules too and found that the formalism presented in this paper satisfy them for $q \to 0$. The computed plasma frequency from equation (24) is plotted in figure 1 as a function of q for a GaAs-QW of $k_F = 5 \times 10^5$ cm^{-1}. Figure 1 shows that inclusion of LFC reduces $\omega_p(q)$ for all values of q. It has been found that $\omega_p(q)$ increases on reducing the width of the QW. It is apparent from equation (17) that the conservation laws relating to $S(q)$ are duly taken care of by the fulfilment of equations (23). The LFC play an important role in determining the physical quantities that involve many body interactions and they also influence the fulfilment of sum-rules. Our computed $G(q)$ from equation (13) is plotted as function of q/k_F in figure 2 for two values of k_F (5×10^6 and 10^6 cm^{-1}) and of a (5 and 10 nm). The $V^0(q)$ used in this paper differs from that used in prior reported work [1, 2], equation (8). Envelope functions that abruptly vanishes at the boundaries of the QW have been used to evaluate $H(\lambda)$ in equation (3), whereas Gaussian type envelope functions have been used to obtain equation (8). We found that our simple approach to compute $G(q)$ provides an adequate representation of LFC in a QW and it agrees with the $G(q)$ computed using the self-consistent quantum mechanical calculation based on the STLS approximation [1, 2] for the values of k_F and a appropriate to a QW. However, for the choice of certain values of k_F and a, our computed $G(q)$ has been

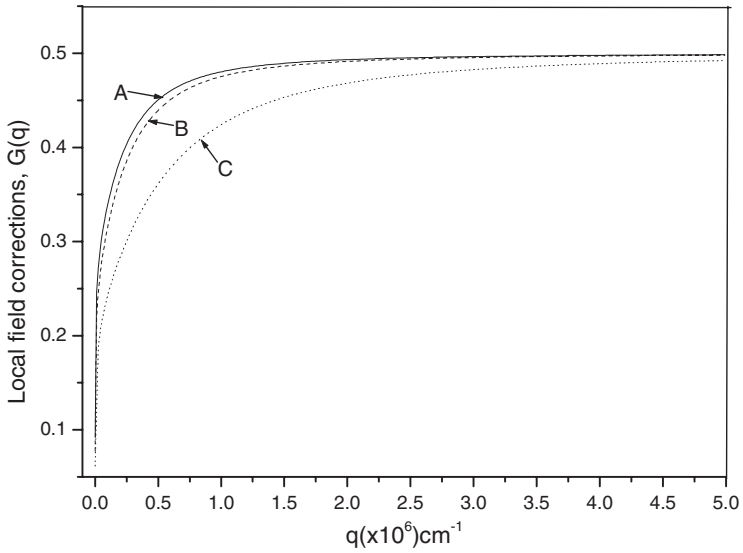

Figure 2. Local field corrections, $G(q)$, are plotted as a function of q. Curve A: $k_F = 5\times10^5$ cm^{-1} and $a = 5$ nm; curve B: $k_F = 5\times10^5$ cm^{-1} and $a = 10$ nm; curve C: $k_F = 10^6$ cm^{-1} and $a = 10$ nm.

found to be smaller than that computed using the STLS approximation [1, 2] at higher values of q. At this juncture, it is difficult to say that the difference in $G(q)$ is due to the different approximations or due to different $V^0(q)$ used in two approaches. Higher $G(q)$ values result in a better fulfilment of sum rules, at higher q values. $G(q)$ exhibits strong q-dependence when q is small ($<2k_F$). It is obvious from the figure 2 that the magnitude of the LFC is enhanced on reducing the width of the QW and reduces on increasing the carrier density. The changes in $G(q)$ on changing a and or changing k_F are more prominent when $0.2 \leqslant q/k_F \leqslant 4$. At higher values of q ($>4k_F$), $G(q)$ becomes almost independent of a and k_F. $G(q)$ is a measure of the strength of the electron–electron interactions that becomes stronger on reducing either the carrier density or a or both, for a QW.

3.1. Structure factor and pair distribution function

An analytical solution of equation (17) with the use of equation (15) is not possible. However, to obtain an analytical result on $S(q)$ without jeopardizing the essential physics, we write $\varepsilon_1(q,\omega)$ in what is known as a plasma pole approximation. The plasma–pole approximation ignores the particle–hole excitations and it assigns the whole spectral weight, dictated by the f-sum rule, to an effective collective plasma excitation, which is assumed to be a real pole of the response function. The phase space restriction on particle–hole excitations increases the spectral weight of the plasma excitation over a wide range of wavevectors and the collective plasma excitation plays a more prominent role in a 1DEG, in contrast to 2D and 3D systems. The plasma–pole approximation indeed works extremely well in calculating a variety of quantities of QW structures [32]. In the plasma pole approximation, $\varepsilon_1(q,\omega) \cong 1 - \omega_p^2(q)/\omega^2$. As has been mentioned before, plasma pole approximation is consistent with conservation laws and the sum rules. The integration over ω, after replacing $\varepsilon_1(q,\omega)$ by $1-\omega_p^2(q)/\omega^2$ in equation (17), yields

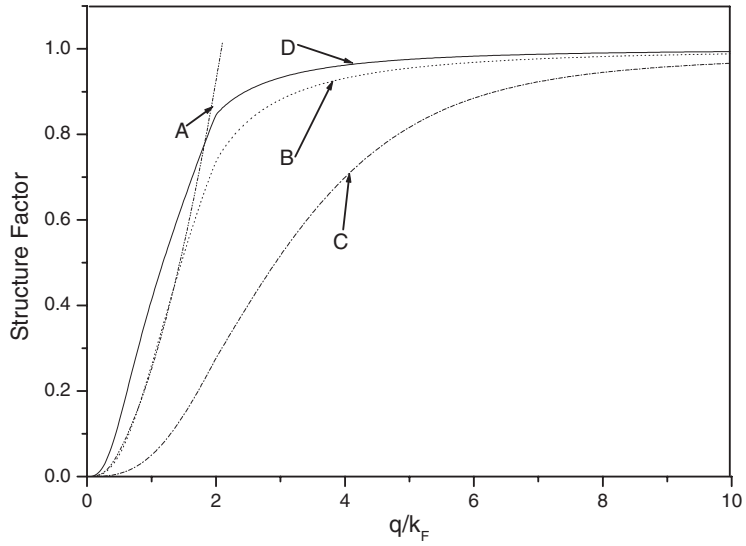

Figure 3. The structure factor, $S(q)$ is plotted as a function of q/k_F at $k_F = 5 \times 10^5$ cm^{-1}. Numerically computed results from equation (17) are displayed for $a = 20$ nm (curve B), $a = 5$ nm (curve C) and $a = 40$ nm (curve D). Analytical results from equation (25) are shown for $a = 20$ nm (curve A).

$$S(z) = \frac{2z^2}{t^2} + \frac{by_0^2(2+t)}{4rt^3}\log\left(\frac{(ty_2^2 + y_0^2 - y_2 r)(ty_1^2 + y_0^2 + y_1 r)}{(ty_1^2 + y_0^2 - y_1 r)(ty_2^2 + y_0^2 + y_2 r)}\right) + \frac{by_0^2(2-t)}{2\sqrt{\Delta}t^3}\left\{\tan^{-1}\left(\frac{2ty_2 + r}{\sqrt{\Delta}}\right) + \tan^{-1}\left(\frac{2ty_2 - r}{\sqrt{\Delta}}\right) - \tan^{-1}\left(\frac{2ty_1 - r}{\sqrt{\Delta}}\right) - \tan^{-1}\left(\frac{2ty_1 + r}{\sqrt{\Delta}}\right)\right\}, \tag{25}$$

where $z = q/k_F$, $b = \frac{m^* V^{\text{eff}}}{zk_F\hbar^2}$, $y_2 = z(z+2)$, $y_1 = z(z-2)$, $t = \sqrt{1+b^2}$, $r = \sqrt{2y_0(1+t)}$, $\Delta = \sqrt{4y_0^2 t - r^2}$, $y_0^2 = (\frac{8z^3}{A-1}) + (z^2+2z)^2$.

We computed $S(z)$ as a function of z using equations (17) and (25) for a GaAs-QW for $k_F = 5 \times 10^5$ cm^{-1}. The integration over ω, in the computation of $S(z)$ from equation (17) with the use of equation (15), has been performed numerically using the Gaussian quadrature formula. Our computed results from equation (17) for three values of a (5, 10 and 20 nm) and from equation (25) for $a = 10$ nm are illustrated in figure 3. The figure exhibits that our simple analytical result, obtained in the plasma pole approximation, shows very good agreement with the detailed numerical result, for $z \leqslant 3/2$. We also computed $S(q, \omega)$, given by equation (17*b*), as a function of ω using $\varepsilon_1(q, \omega)$ obtained from equation (15*a*) and from the plasma pole approximation. Two results exhibit excellent agreement with each for $z \leqslant 3/2$. It is manifestation of the following: (i) in a QW, the prohibition of particle–hole excitations from a large portion of the low energy phase space, which arises from the momentum–energy conservation, increases the dominance of plasma excitations, and (ii) the oscillator strength of the plasma excitations in a QW extends well into the range of large wavevectors and it decreases slowly with increasing wavevector [10, 32]. The figure also displays that the structure factor declines on reducing the width of a QW, at all values of q. We find, however, that the increase in $S(q)$ is not proportional to a and it tends to saturate for larger values of a, at a given q-value.

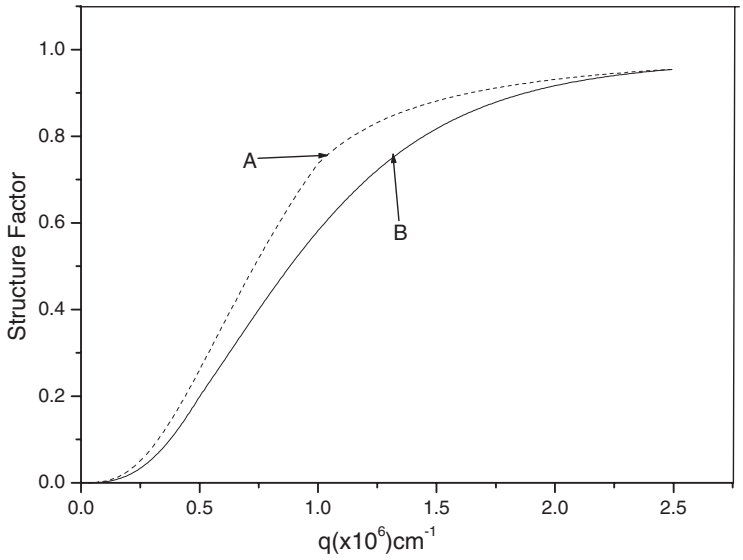

Figure 4. Computed structure factor, $S(q)$, as a function of q at $a = 20$ nm. Numerically computed results are depicted for $k_F = 2.5 \times 10^5$ cm^{-1} (curve A) and $k_F = 5 \times 10^5$ cm^{-1} (curve B).

The effect of change in carrier density on the structure factor can be seen from figure 4, where $S(q)$ is plotted as a function of z for two values of k_F (2.5×10^5 and 5×10^5 cm^{-1}) at $a = 20$ nm. $S(q)$ declines on increasing the carrier density, for given values of q and a, as is obvious from figure 4. The prior reported calculations on $S(q)$ had been made by solving numerically the simultaneous equations for $S(q)$, $G(q)$ and $\chi(q, \omega)$, as their definitions are inter-dependent in the STLS approximation [1, 2]. On the other hand, in our approach $S(q)$, $G(q)$ and $\chi(q, \omega)$ are defined and computed independent of each other. This greatly simplified the computation task and also enabled us to provide analytical results on $S(q)$ within the plasma pole approximation. The computed $S(q)$, as a function of q, from our simple approach shows very good agreement with the prior reported work [1, 2, 10], however.

We computed numerically equation (18) with the use of equation (17) for two values of a (20 and 10 nm) at $k_F = 5 \times 10^5$ cm^{-1} and with the use of equation (25) for $k_F = 5 \times 10^5$ cm^{-1} and $a = 20$ nm. Our computed $g(r)$ is displayed as a function of $k_F r$ in figure 5. It is evident from the figure that the computed $g(r)$ with the use of analytically calculated $S(q)$ is in reasonably good agreement with the $g(r)$ computed using numerically computed $S(q)$. We thus find that the many body effects in a QW are well described by our simple analytical result given by equation (25). Our computed results on $g(r)$ suggest that on decreasing the width of QW for fixed k_F, the average distribution of electrons about an electron enhances at larger r-values and it becomes negative at smaller values of r. The IRPA fails to describe $g(r)$ when $g(r)$ becomes negative. This has also been observed in the calculations of $g(r)$ using the STLS approximation [1, 2]. We also computed $g(r)$ as function of r for different values of k_F and found that an increase in carrier density leads to the reduction at larger r-values and enhancement at smaller values of r, in the average distribution of electrons about an electron in a QW of fixed a.

3.2. Dielectric function and screened potential

We computed $W(q)$ as function of q using equation (19) for $a = 20$ nm and $k_F = 5 \times 10^5$ cm^{-1}. Our computed IRPA and RPA results are compared with the TFA results. The screened impurity

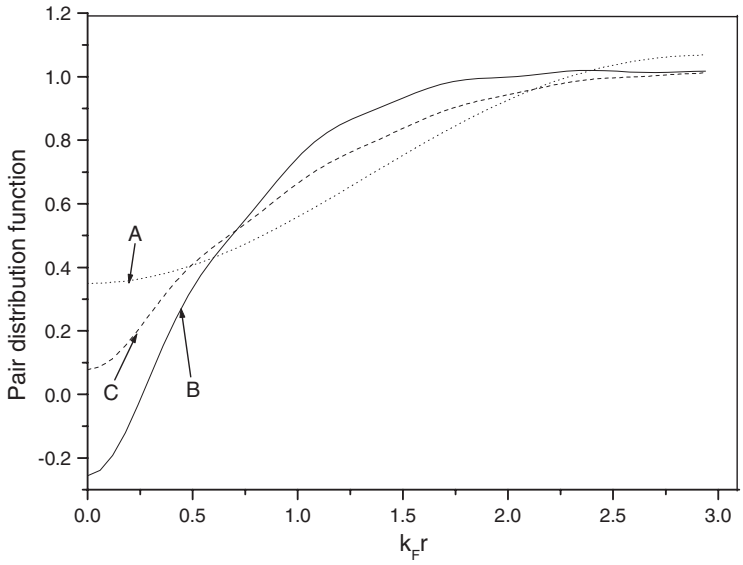

Figure 5. The pair distribution function, $g(r)$, from equation (18) is plotted as a function of $k_F r$ at $k_F = 5 \times 10^5$ cm^{-1}. Computed results are displayed using analytical calculated $S(q)$ at $a = 20$ nm (curve A), and with the use of numerically computed $S(q)$ from equation (17) for $a = 10$ nm (curve B) and for $a = 20$ nm (curve C).

potential within TFA is given by [25]

$$W_{\rm TF}(q) = \frac{-2Ze^2 \ln(qa)}{1 - q_{\rm s} \ln(qa)}, \tag{26}$$

where $q_{\rm s} = 4/\pi k_{\rm F} a_0$. The $a_0 = \hbar^2/m^* e^2$ is the Bohr radius. The TFA is valid only for smaller values of $q < (k_{\rm F})$. Our computed normalized screened potential, $W(q)/Z\varepsilon_{\rm F}$, from equations (19) and (26), is shown in figure 6 as a function of z when $0 \leqslant z \leqslant 2.5$. The TFA is valid only for small values of $z(\ll 2)$ and the TFA results go over to RPA results for $z \to 0$, as is seen from the figure. The TFA-SP, as compared to IRPA-SP and RPA-SP, declines more rapidly with z and it overestimates the screening effects for z not close to zero. Interesting features such as Friedel oscillations, which are a manifestation of logarithmic divergent behaviour of SP at around $z = 2$ and dominate the long-range behaviour of SP, cannot be exhibited by $W_{\rm TF}(q)$. The logarithmic divergent behaviour at around $z = 2$ in computed $W(q)/Z\varepsilon_{\rm F}$ using IRPA and RPA can clearly be seen from equation (15*a*) and figure 6. Though the overall behaviour of the screened potential for a QW is found similar to that of 2D free electron gas, the behaviour at z-values close to $z = 2$ is found to be more pronounced in the case of a QW. This suggests more pronounced Friedel oscillations in a QW, as compared to 2D free electron gas. We computed IRPA $W(q)/Z\varepsilon_{\rm F}$ and its discrete Fourier transform by taking several values of sampling interval, $\Delta = z/N$, for a fixed value of the number of sample points, $N = 1024$. The ith value of z, z_i is given by $i\Delta$, with $0 \leqslant i \leqslant N$. The choice of Δ determines the range of z for which $W(q)/Z\varepsilon_{\rm F}$ is computed. Our computed normalized discrete Fourier transforms of $W(q)/Z\varepsilon_{\rm F}$, termed as $W(j)/Z\varepsilon_{\rm F}k_{\rm F}$, are plotted as a function of j in figure 7, for three values of Δ (0.004, 0.1 and 0.4) at $k_{\rm F} = 5 \times 10^5$ cm^{-1} and $a = 20$ nm. The j is a discrete Fourier variable corresponding to i. The computed $W(j)/Z\varepsilon_{\rm F}k_{\rm F}$ for $\Delta = 0.004$ exhibits oscillatory behaviour which is more pronounced at smaller values of $j(<20)$, as is seen from figure 7. For $\Delta = 0.004$, z varies between 0 and 4. On increasing Δ, the period of oscillations increases

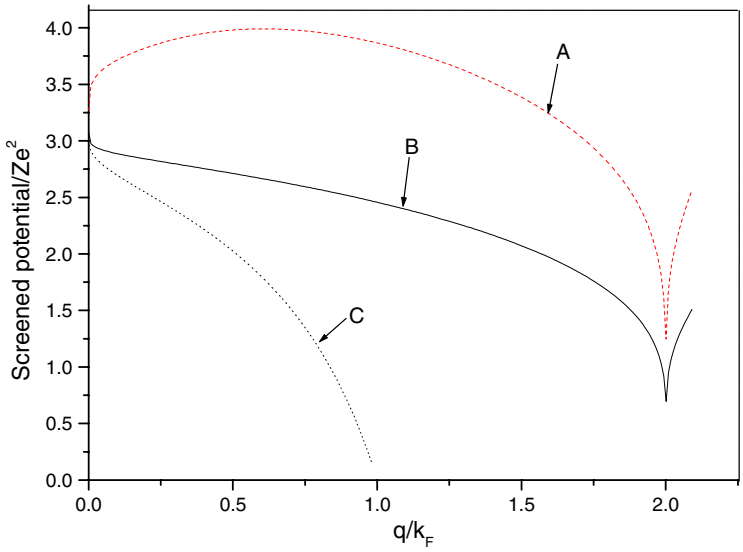

Figure 6. The normalized screened potential in Fourier space is shown as a function of q/k_{F} using the improved random phase approximation (curve A), the random phase approximation (curve B) and the Thomas–Fermi approximation (curve C).

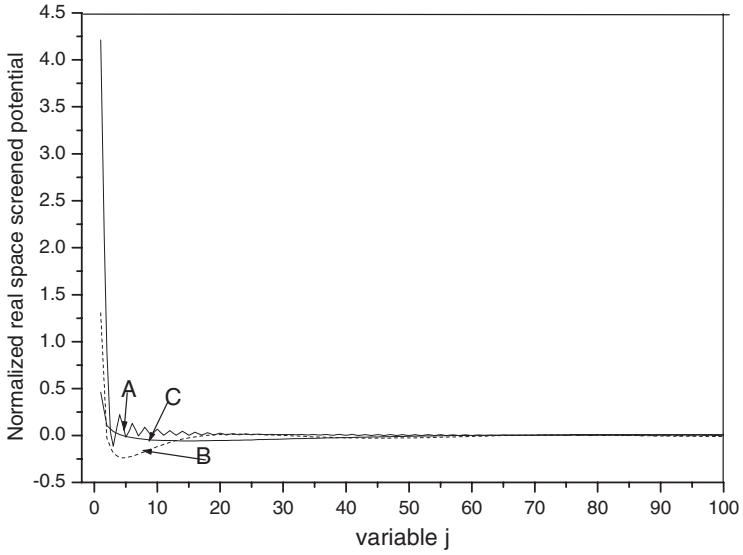

Figure 7. The normalized discrete real space screened potential, $W(j)/Z\varepsilon_{\mathrm{F}}k_{\mathrm{F}}$, is displayed as a function of j for different values of sampling parameter (Δ) at fixed number of points, $N = 1024$, $k_{\mathrm{F}} = 5 \times 10^5$ cm^{-1} and $a = 20$ nm. Results are shown for $\Delta = 0.004$ and $0 \leqslant z \leqslant 4.08$ (curve A), $\Delta = 0.1$ and $0 \leqslant z \leqslant 102$ (curve B), and $\Delta = 0.1$ and $0 \leqslant z \leqslant 408$ (curve C).

and the oscillations in the range of $0 \leqslant j \leqslant 100$ almost disappear when $\Delta > 0.1$, as exhibited in the figure. Also, it is to be noted that the magnitude of $W(j)/Z\varepsilon_{\mathrm{F}}k_{\mathrm{F}}$ decreases on enhancing Δ for j close to zero. Our computed $W(j)/Z\varepsilon_{\mathrm{F}}k_{\mathrm{F}}$ for two values of a (20 and 4 nm) and $k_{\mathrm{F}} = 5 \times 10^5$ cm^{-1} is plotted in figure 8. As is apparent from the figure, the magnitude of the

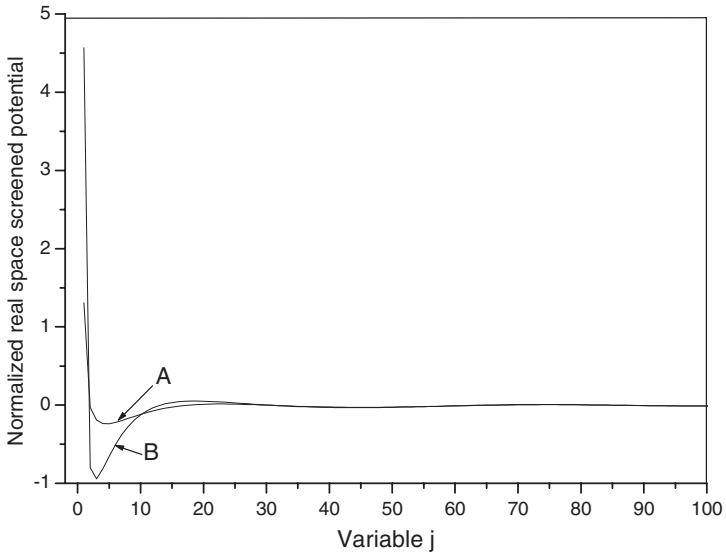

Figure 8. The normalized discrete real space screened potential, $W(j)/Z\varepsilon_F k_F$, is plotted as a function of j when $\Delta = 0.1$ and $N = 1024$ for $a = 20$ nm (curve A), and for $a = 4$ nm (curve B) at $k_F = 5 \times 10^5$ cm^{-1}.

screened potential enhances on reducing the width of QW at all values of r and it diverges for $r \to 0$ in a QW of fixed carrier density.

3.3. Density of the screening charge

The $n_s(r)$ has the dimension of charge per unit length in the case of a QW. Our computed $n_s(r)/Zek_F$, within the IRPA and RPA is plotted as a function of $k_F r$ in figure 9 for a QW of $a = 20$ nm and $k_F = 5 \times 10^5$ cm^{-1}. The Friedel oscillations are also seen in $n_s(r)/Zek_F$. The inclusion of LFC reduces the magnitude of $n_s(r)/Zek_F$ at all r-values and makes it better behaved for $r \to 0$, as is obvious from figure 9. Unlike the screened potential of a point charge, the density of the screening charge remains finite even for $r \to 0$, as is obvious from equation (21) and figure 9.

3.4. Exchange energy and IRPA self-energy

Analytical results on $E^{xc}(k)$ with the use of $V^{eff}(|\mathbf{k} - \mathbf{k}'|)$, given by equation (11), are not possible. However, simple analytical results for $E^{xc}(k)$ can be obtained on replacing $V^{eff}(|\mathbf{k} - \mathbf{k}'|)$ by $V^0(|\mathbf{k} - \mathbf{k}'|)$ defined by equation (7). Evaluation of equation (7) on taking $1/a$ as the upper limit of integration gives

$$V^0(|\mathbf{k} - \mathbf{k}'|) = \frac{e^2}{\varepsilon_0} \log\left[\frac{\sqrt{(k-k')^2a^2+1}+1}{\sqrt{(k-k')^2a^2+1}-1}\right]. \tag{27}$$

On replacing $V^{eff}(|\mathbf{k} - \mathbf{k}'|)$ by equation (27), and then performing integration over k', we obtain

$$E^{xc}(k) = \frac{e^2}{2\pi a\varepsilon_0}\left[x_1 \log\left(\frac{\sqrt{x_1^2+1}+1}{\sqrt{x_1^2+1}-1}\right) - x_0 \log\left(\frac{\sqrt{x_0^2+1}+1}{\sqrt{x_0^2+1}-1}\right) + 2\log\left(\frac{\sqrt{x_1^2+1}+x_1}{\sqrt{x_0^2+1}+x_0}\right)\right], \tag{28}$$

where $x_1 = (k + k_F)a$ and $x_0 = (k - k_F)a$.

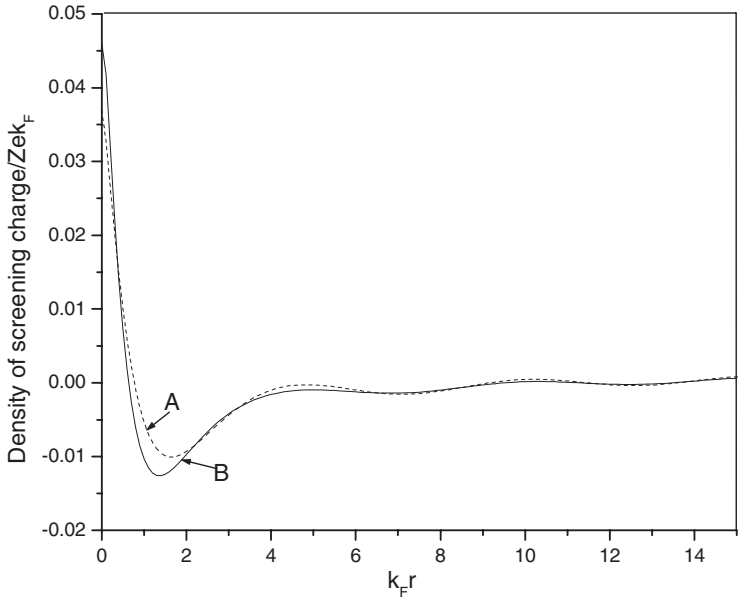

Figure 9. The normalized density of the screening charge is shown as a function $k_F r$ using the IRPA (curve A) and the RPA (curve B) at $k_F = 5 \times 10^5$ cm^{-1} and $a = 20$ nm.

We computed the dimensionless exchange energy, $\pi E^{xc}(k)/e^2 k_F$, as a function of k/k_F from equation (22*a*) with the use of equation (11) and from equation (28) for three values of a (5, 10 and 20 nm) and $k_F = 5 \times 10^5$ cm^{-1}. Our computed results are displayed in figure 10. The figure makes it clear that the simple analytical result given by equation (28) shows good agreement with the detailed numerical result that includes the LFC. The agreement between analytical and numerical results is very good when the width of the QW is around 10 nm. The exchange energy enhances on decreasing the width of the QW. The computed exchange energy is smooth at all values of k except for the discontinuity of its derivative at $k = k_F$. We also computed the exchange energies of 2D and 3D electron gas and found that the exchange energy of the QW is larger than that of 2D, which in turn is larger than that of 3D-electron gas. This is in accordance with the well-known fact that the strength of exchange interactions enhances on reducing the dimensionality of the system.

An analytical solution of equation (22*b*) is not possible even if we replace $V^{eff}(|\mathbf{k} - \mathbf{k}'|)$ by equation (27). We computed $E^{sl}(k)$ from equation (22*b*) with the use of equation (10) for two values of a (5 and 20 nm) and two values of k_F (5×10^5 and 10^6 cm^{-1}). Our computed $\pi E^{sl}(k)/e^2 k_F$ is plotted as a function of k/k_F in figure 11. The overall behaviour of $E^{sl}(k)$ is similar to that of $E^{xc}(k)$. However, on comparing figures 10 and 11 it is interesting to note that the magnitude of $E^{sl}(k)$ is roughly ten times smaller than that of $E^{xc}(k)$, at a given k-value. Similar to the case of a 3D-electron gas, both $E^{xc}(k)$ versus k curves and $E^{sl}(k)$ versus k curves exhibit steep change at around $k = k_F$. Figure 11 shows that the IRPA self-energy enhances on reducing the width and increasing the carrier density in a QW. We also computed $E^{sl}(k)$ without LFC. As is obvious from figure 11, inclusion of LFC brings down the magnitude of the screened exchange energy at all values of k. We also computed the normalized screened exchange energy versus normalized wavevector for 3D and 2D electron gas and compared them with the corresponding results of a QW. Similar to the case of exchange energy, the screened exchange energy is also found to decline on increasing the dimensionality of the

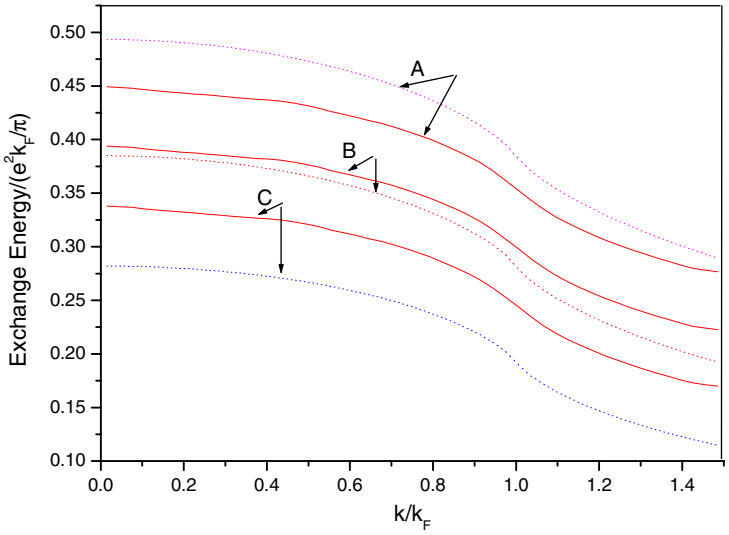

Figure 10. The normalized exchange energy, $\pi E^{\rm xc}(k)/e^2k_{\rm F}$ is plotted as function of $k/k_{\rm F}$ at $k_{\rm F} = 5 \times 10^5$ cm^{-1} for $a = 5$ nm (curves A), $a = 10$ nm (curves B), and $a = 20$ nm (curves C). Dot–dot curves display analytical results from equation (28), whereas solid line curves are numerically computed results from equation (22*a*).

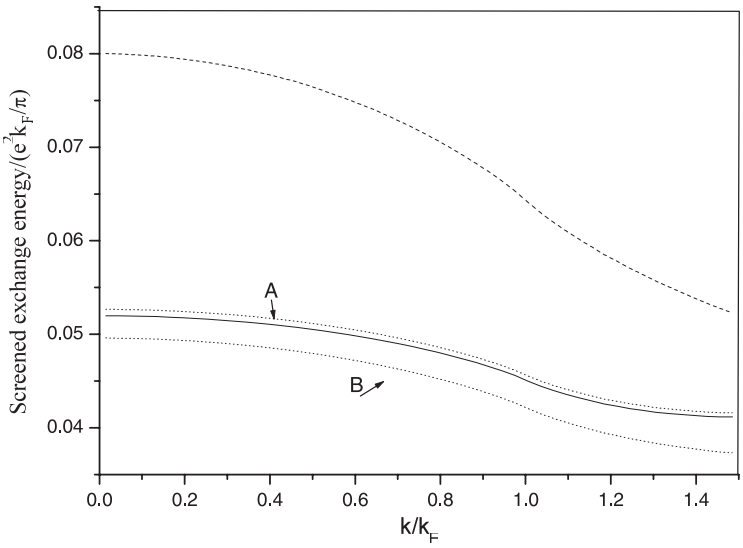

Figure 11. The normalized self-energy, $\pi E^{\rm sl}(k)/e^2k_{\rm F}$, is shown as a function of $k/k_{\rm F}$ from equation (22*b*). The IRPA results are depicted for $k_{\rm F} = 10^6$ cm^{-1} and $a = 20$ nm (dash–dash curve), $k_{\rm F} = 5 \times 10^5$ cm^{-1} and $a = 20$ nm (dot–dot curve B), $k_{\rm F} = 5 \times 10^5$ cm^{-1} and $a = 5$ nm (solid curve). The RPA results are shown by dot–dot curve A at $k_{\rm F} = 5 \times 10^5$ cm^{-1} and $a = 20$ nm.

system. It has also been found that the IRPA self-energy almost doubles on going from 3D to 2D or from 2D to 1D electron gas. The large value of IRPA self-energy in the case of a 1D system, as compared to 3D and 2D systems, is the manifestation of weaker screening effects and smaller carrier density (Fermi energy) in a 1D system. Our investigations thus suggest

that contribution from electron–electron interactions to the single particle energy increases on reducing the effective dimensions of a system and the use of the Fermi-liquid approach could not be justified in describing some of the single particle properties of a 1D system without significant impurity concentration. This could be seen in accordance with the viewpoint that a Luttinger liquid model, as compared to a Fermi liquid model, can be more suitable to describe the electronic properties of an impurity free 1D system.

4. Conclusions

We calculated the $S(q)$, $g(r)$, $W(q)$, $W(j)$, $n_s(r)$, $E^{xc}(k)$ and $E^{sl}(k)$ for a QW using an IRPA that incorporates the LFC within the Hubbard approximation. Our formalism complies with conservation laws and sum-rules. The numerical results are displayed for a GaAs-QW. Analytical results are also obtained on $S(q)$ within a plasma pole approximation and on $E^{xc}(k)$ using a bare coulomb potential that describes well interactions at distances larger than the width of the QW. The analytical results show good agreement with detailed numerical results. At all q values, $S(q)$ declines on reducing a and increasing k_F. The rate of decline is higher at smaller q-values than that at larger values of q. The computed $S(q)$, as a function of q, from our simple approach shows very good agreement with the prior reported work using the STLS approximation. On decreasing the width of the QW with fixed k_F, $g(r)$ enhances at larger r-values, and becomes negative at smaller values of r. This suggests the failure of the IRPA in describing $g(r)$ at smaller values of r on reducing the width of QW. Prior reported calculations of $g(r)$, using the STLS approximation, also exhibit negative values of $g(r)$ at smaller values of r [1, 2]. Both computed SP and $n_s(r)$ exhibit the Friedel oscillations. The magnitude of SP enhances on reducing the width of the QW at all values of r, for fixed carrier density and it diverges for $r \to 0$. Our calculations of $E^{xc}(k)$ and $E^{sl}(k)$ suggest that contribution from electron–electron interactions to the single particle energy enhances on reducing the effective dimensions of a system and the use of the Fermi-liquid approach may not be justified in describing some of the single particle properties of a 1D system without significant impurity concentration.

Acknowledgment

Authors acknowledge with thank the financial support from the department of science and technology, government of India, through a research project, to carry out this work.

References

[1] Tas M and Tomak M 2003 *Phys. Rev.* B **67** 235314
[2] Tanatar B and Bulutay C 1999 *Phys. Rev.* B **59** 15019
[3] Thakur J S and Neilson D 1997 *Phys. Rev.* B **56** 4679
[4] Hu B Y-K and Das Sarma S 1993 *Phys. Rev.* B **48** 5469
Hu B Y-K and Das Sarma S 1992 *Phys. Rev. Lett.* **68** 1750
[5] Wang D W, Millis A J and Das Sarma S 2001 *Phys. Rev.* B **64** 193307
[6] Bulutay C and Tomak M 1996 *Phys. Rev.* B **53** 7317
[7] Moudgil R K, Ahluwalia P K and Pathak K N 1995 *Phys. Rev.* B **52** 11945
[8] Wang D W and Das Sarma S 2001 *Phys. Rev.* B **65** 35103
[9] Schuck P, Schulze H J, Giai N V and Zverev M 2003 *Phys. Rev.* B **67** 233404
[10] Agosti D, Pederia F, Lipparini E and Takayanagi K 1998 *Phys. Rev.* B **57** 14869
[11] Calmels L and Gold A 1995 *Phys. Rev.* B **52** 10841
[12] Das Sarma S and Hwang E H 2004 *Phys. Rev.* B **69** 195305

[13] Lilly M P, Reno J L, Simmons J A, Spielman I B, Eisenstein J P, Pfeiffer L N, West K W, Hwang E H and Das Sarma S 2003 *Phys. Rev. Lett.* **90** 056806
[14] Sólyom J 1979 *Adv. Phys.* **28** 201
[15] Voit J 1995 *Rep. Prog. Phys.* **58** 977
[16] Haldane F D H 1981 *J. Phys. C: Solid State Phys.* **14** 2585
[17] Kramer B and Sassetti M 2000 *Phys. Rev.* B **62** 4238
[18] Hãusler W, Kecke L and MacDonald A H 2002 *Phys. Rev.* B **65** 085104
[19] Lee J, Eggert S, Kahng S-J, Shinohara H and Kak Y 2004 *Phys. Rev. Lett.* **93** 166403
[20] Wang D-W, Mills A J and Das Sarma S 2004 *Phys. Rev.* B **70** 165101
[21] Rauf H, Picher T, Knupfer M, Fink J and Kataura H 2004 *Phys. Rev. Lett.* **93** 096805
[22] Goñi A R, Pinczuk A, Weiner J S, Calleja J M, Dennis B S, Pfeiffer L N and West K W 1991 *Phys. Rev. Lett.* **67** 3298
[23] Liu D Z, Hu B Y-K, Stafford C A and Das Sarma S 1994 *Phys. Rev.* B **50** 5799
[24] Holas A and Rahman S 1987 *Phys. Rev.* B **35** 2720
[25] Reyes J A and Massot M D C 1998 *Phys. Rev.* B **57** 9869
[26] Lee J and Spector H N 1984 *J. Appl. Phys.* **57** 366
[27] Sharma A C and Ashraf S S Z 2004 *J. Phys.: Condens. Matter* **16** 3117
[28] Sharma A C and Bajpai A 2002 *Int. J. Mod. Phys.* B **16** 1511 and references therein
[29] Li Q P and Das Sarma S 1991 *Phys. Rev.* B **43** 11768
[30] Mahan G D 1990 *Many Particle Physics* 2nd edn (New York: Plenum)
[31] Ayaz Y 2003 *Phys. Rev.* B **67** 075410
[32] Das Sarma S, Hwang E H and Zheng L 1996 *Phys. Rev.* B **54** 8057